# Development of oxide dispersion strengthened 2205 duplex stainless steel composite

Oladayo OLANIRAN[1, 2*], Peter Apata OLUBAMBI[1], Benjamin Omotayo ADEWUYI[1], Joseph Ajibade OMOTOYINBO[1], Ayodeji Ebenezar AFOLABI [1], Davies FOLORUNSO [1], Adekunle ADEGBOLA[3], and Emanuel IGBAFEN[1]

[1] *Chemical and Metallurgy Department, Tshwane University of technology, Pretoria, South Africa.*
[2] *Metallurgical and Materials Engineering Dept., Federal University of technology, Akure, Nigeria.*
[3] *The polytechnic, Mechanical Engineering Department, Ibadan, Nigeria.*
E-mails: oladayolaniran@gmail.com, olubambipa@tut.ac.za, tayo_adewuyi@yahoo.com, jaooyinbo@futa.edu.ng, ayode86@yahoo.com, stdavies@yahoo.com, kunleade@yahoo.com, igbafene@futa.edu.ng
[*] Corresponding author, phone: +2348035001939

**Abstract**

Composites of duplex stainless steel were produced by oxide dispersion strengthening with comparatively improved mechanical properties by hot press sintering of partially stabilized Zirconia (PSZ, 3% yttria, mole fraction) dispersion in 2205 duplex stainless steels. Ceramic oxide was added as reinforcement, while chromium (Cr) and Nickel (Ni) were incorporated to maintain the austenitic/ferritic phase balance of the duplex stainless steel. The powders and sintered were characterized in detail using scanning electron microscopy (SEM) and X-ray diffraction (XRD). The microstructural evolution and phase formation during oxide dispersion strengthening of duplex stainless steel composites were investigated. The influence of composition variation of the reinforcements on the microstructural and corrosion behaviour in simulated mine water of the composites were investigated. In this manuscript, it was established that composition has great influence on the structure/properties relationship of the composites developed.

**Keywords**

Strengthening; Metal-matrix; Sintering; Corrosion; Composites

## Introduction

Powder metallurgy allows composite materials, notably metal–ceramic composites, to be produced by sintering a mixture of powders. It consists in consolidating powder mixture by successive pressing and sintering or hot pressing [1]. The densification of metal–ceramic powder mixture during hot pressing has been largely studied. It has been shown in particular that particle size ratio has a prominent effect on the densification kinetics. The final density plays a major role on the mechanical properties of the sintered composite; it is important to have it as high as possible [2-5]. Experimental studies about densification of powder mixtures during sintering have been undertaken by different researchers. However, Olmos et al, 2009 [1] in their study, demonstrated that a very small amount of inclusion (typically 3 vol. %) can significantly affect the densification which has been attributed to different phenomena such as inclusion induced stress, heterogeneity and network formation.

Nanocrystalline materials have attained great scientific interests in recent years because they possess superior mechanical, physical and chemical properties compared to conventional coarse–grained materials [25]. Nanostructured solids with dispersion strengthening offered by uniform distribution of nano-intermetallic or nano-ceramic phases are extremely useful for structural applications at ambient or elevated temperatures. Ceramic oxide dispersion strengthened steel find wide applications in fabricating discs and other critical parts of jet engines, pump bodies and parts, nuclear fuel element spacers etc. Nano–$Y_2O_3$ dispersed steel possess a combination of body cantered cubic (BCC) structure with low coefficient of thermal expansion, high thermal conductivity, good creep resistance and high tensile/compressive strength as reported by Karak et al., 2010 [4] and Glage et al., 2014 [6].

Ceramic reinforcement with zirconia can exist in three forms; cubic, tetragonal and monoclinic. Transformation from the tetragonal to the monoclinic modification is followed by a volume change resulting in catastrophic fracture and hindering the application of pure $ZrO_2$ composites. Stabilizers such as $Y_2O_3$, CaO, MgO allow the stabilization down to room temperature [6]. Zirconia stabilized with 3mol % yttria was selected for its particular mechanical and thermal properties such as its high melting point, high hardness, high electrical conductivity, excellent corrosion resistance against molten iron and slag, high thermal shock resistance. These properties make it an excellent candidate for very high temperature applications as in combustion chambers, thermal protection shields for space vehicles etc. [7,8].

Mechanical alloying is a useful technique to synthesize novel materials including nanostructured and amorphous products in powder form, consolidation of such powders into a bulk component without deteriorating or destroying the as–milled novel mictrostructural state poses a genuine challenge. Various attempts that have achieved reasonable success in this regard are high pressure sintering, equi–channel angular pressing, laser sintering, pulse plasma sintering and hot isostatic pressing as reported by Karak [4].

## Material and method

Mixture of atomized polycrystalline 2205 supplied be WEARTECH Ltd., South Africa with composition presented in Table 1, partially stabilized Zirconia (PSZ, 3%yttria, mole fraction), chromium and Nickel were used in this study.

Table 1. Elemental composition of as-received 2205 powders

| Cr (%) | Ni (%) | Mo (%) | Si (%) | N (%) | P (%) | C (%) | Mn (%) | S (%) |
|---|---|---|---|---|---|---|---|---|
| 22.8 | 5.1 | 3.3 | 0.77 | 0.25 | 0.014 | 0.012 | 0.98 | 0.006 |
| Al (%) | Co (%) | Cu (%) | P (%) | Sn (%) | Ti (%) | W (%) | B (%) | Fe (%) |
| - | - | - | - | - | - | - | - | Balance |

The powders particle sizes as stated by the suppliers are: Duplex stainless steel (2205) - 22µm, partially stabilized Zirconia (PZY) is 50nm; chromium and Nickel are -325 mesh and 4.5µm respectively. XRD was used to determine the phase present. Different composites were produced by weighing different percentages of the matrix, the reinforcement and the alloying elements as indicated in Table 2.

Table 2. Powder composition of Duplex stainless steel 2205 composites

| Sample no | 2507 Composition % | $ZrO_2(Y_2O_3)$ % | Cr % | Ni % |
|---|---|---|---|---|
| X | 100 | - | - | - |
| A1 | 99.5 | 0.5 | - | - |
| A2 | 98.5 | 0.5 | 0.815 | 0.185 |
| A3 | 97 | 1 | 1.63 | 0.37 |
| A4 | 95 | 2 | 1.63 | 0.37 |
| A5 | 95 | 3 | 2.44 | 0.36 |

These weighed powders were mixed in the TUBULA® mixer for 2 hours, after which the

admixed powders were sintered in a hot press; High Temperature High Pressure (HTHP) at sintering temperature of 1100$^{o}$C, pressure of 30 MPa and 30 minutes holding time using Argon gas flow to achieve a consolidated bulk cylindrical composite of 18 mm diameter and 2 mm thickness.

Scanning electron microscope (SEM) with a link energy dispersive X-ray spectroscopy (EDS) detector attachment, model JEOL, JSM–7600F, were used to assess shape of agglomeration of particles and the compositions of the various ODS composite. The SEM images were analysed at 500 microns. The as-received 2205 was characterized, also are the admix powders. The compositions were processed by the EDS spectrum. The Phase identification was determined using X-ray diffraction PANanalytical X'pert PRO with Co anode, step size of 2θ (generating settings 30 kv, 10 mA).

The densities of the sintered samples were measured using Archimedes principle after weighing in air and water separately using an electronic balance of 0.01mg precision. Morphology, shape and size distribution of the phases in the sintered components were studied using a field emission scanning electron microscopy (FESEM). Relative density was calculated from the sintered density and theoretical density, the latter was deduced from the simple law of mixture; $\rho_t=\rho_1 f_1+\rho_2 f_2+ \ldots + \rho_n f_n$, where ρi and fi are the theoretical density and the volume fraction of component i.

Vickers hardness were obtained for the sintered samples. The hardness test was carried out under an indenter load of 0.1Hv and dwell time of 15 seconds.

Potentio-dynamic polarization experiment was carried out to study the electrochemical behaviour of the sintered DSS composites in both simulated mine water and 3.5% NaCl solution. The polarization curves were obtained at the same conditions after 25 minutes of the composite immersion in simulated mine water at room temperature. Values of corrosion potentials, corrosion current densities and corrosion rates were calculated from polarization curves.

## Results

A representative microstructural characterization of the powders and the sintered composites are presented in Figures 1 and 2, while the phase analysis is represented in Figure

3.

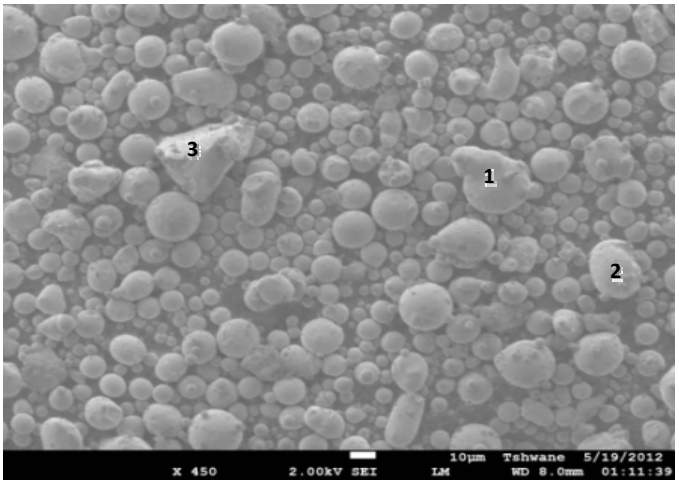


***Figure 1.*** *Typical SEM image and EDS spot analysis of admix powder*

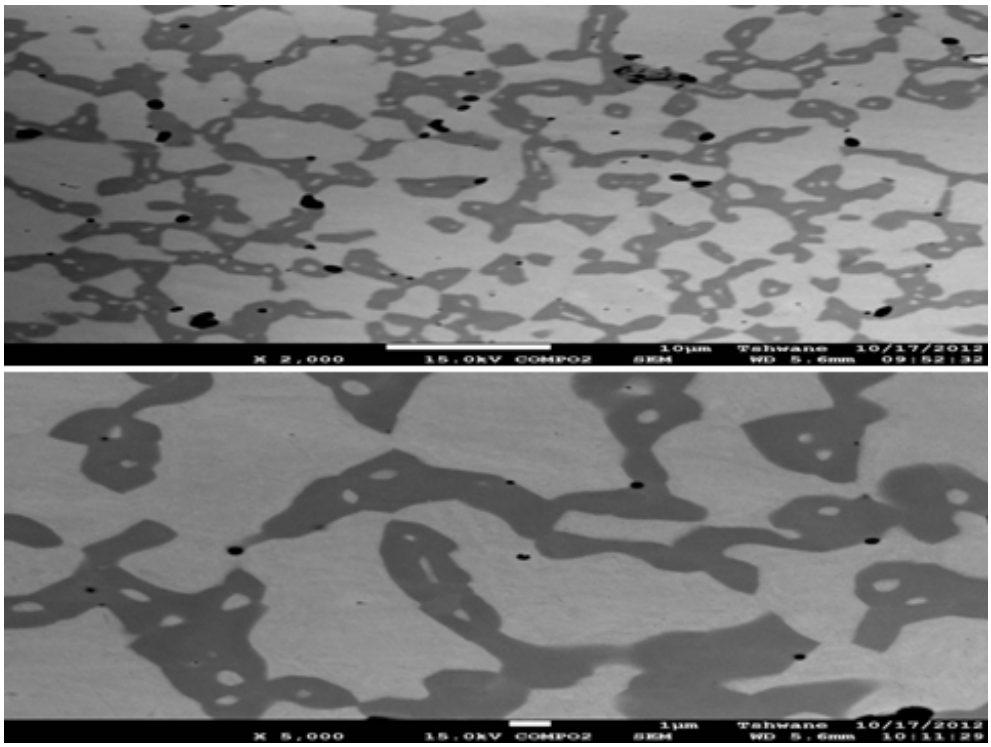


***Figure 2.*** *Typical SEM micrograph of sintered composite at different magnification*

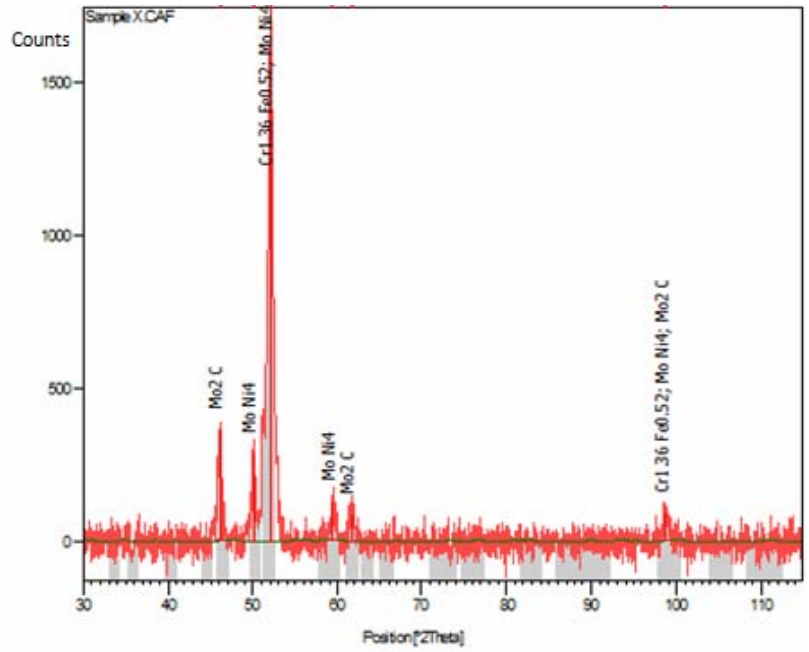


***Figure 3.*** *XRD showing phase analysis of a typical sintered DSS composite*

Densification properties are presented in Table 3while percentage densification of the sintered composites is represented in Figure 4.

Table 3. Properties of hot pressed DSS composites

| Sample | Density [g/cm$^3$] | Theoretical [g/cm$^3$] | Relative density [%] | Open porosity (%) | Vickers Hardness Value (Hv0.1) |
|---|---|---|---|---|---|
| X | 7.72 | 7.7 | 99.6 | 0.4 | 847.01 |
| A1 | 7.68 | 7.73 | 99.35 | 0.65 | 916.13 |
| A2 | 7.67 | 7.71 | 99.48 | 0.52 | 845.02 |
| A3 | 7.69 | 7.72 | 99.51 | 0.49 | 852.11 |
| A4 | 7.64 | 7.69 | 99.5 | 0.5 | 881.02 |
| A5 | 7.62 | 7.66 | 99.53 | 0.4 | 835.02 |

Figures 4 and 5 represent the open circuit potential and polarization curve respectively for the corrosion measurement. The anodic polarization, cathodic polarization and the corrosion rate in mm/year are represented in Table 4. Microstructural examinations conducted on the corroded samples is typically represented in Figure 6.

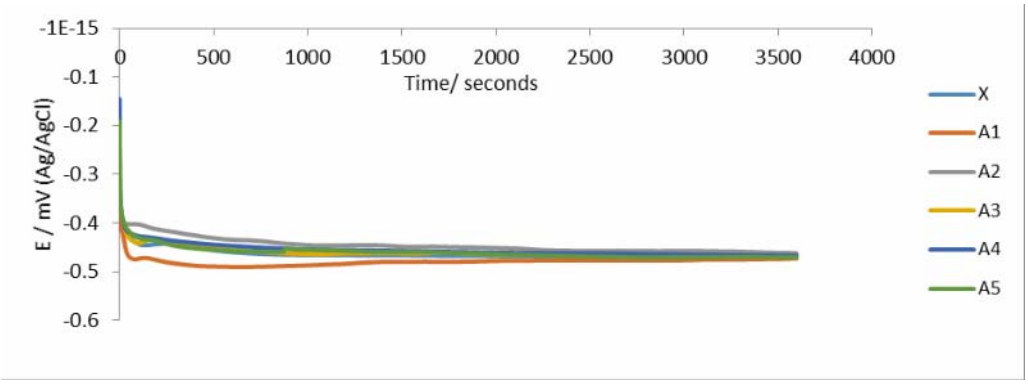


***Figure 4.*** *OCP measurement for 2205 DSS composites in simulated mine water*

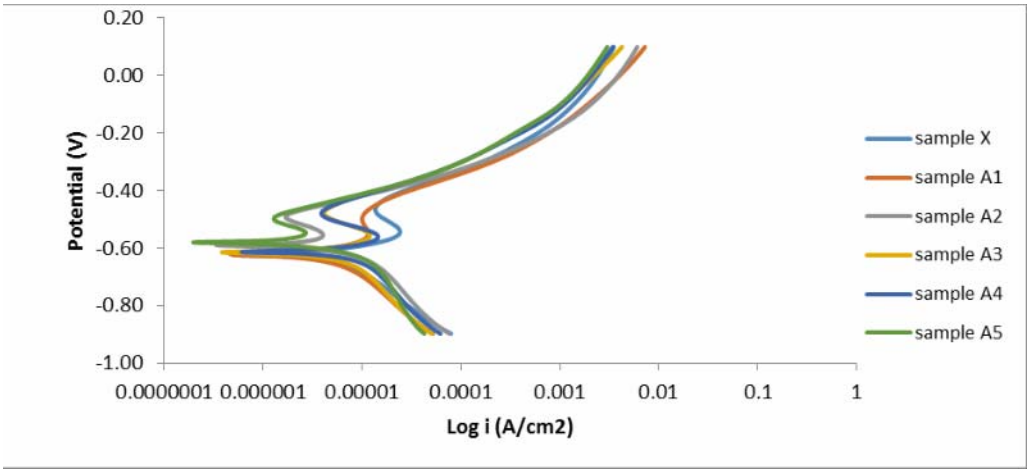


***Figure 5.*** *Polarization curves of PM 2205 duplex stainless steel composite in simulated Mine water*

Table 4. Corrosion rate of 2205 DSS composites in simulated mine water

| Sample | Ecorr | icorr(A) | Icorr(A/cm$^2$) | bc(v/dec) | ba(v/dec) | Rp(Ω) | Cr(mm/yr) |
|---|---|---|---|---|---|---|---|
| X | -0.628 | 5.82E-6 | 4.096E-6 | 0.116 | 0.229 | 1.972E3 | 4.844E-2 |
| A1 | -0.625 | 2.57E-6 | 2.545E-6 | 0.082 | 0.101 | 1.397E3 | 3.024E-2 |
| A2 | -0.595 | 1.70E-6 | 1.487E-6 | 0.086 | 0.035 | 7.573E2 | 1.769E-2 |
| A3 | -0.617 | 3.55E-6 | 2.793E-6 | 0.088 | 0.124 | 1.335E3 | 3.307E-2 |
| A4 | -0.619 | 6.05E-6 | 4.767E-6 | 0.138 | 0.161 | 1.586E3 | 5.657E-2 |
| A5 | -0.583 | 7.13E-7 | 5.612E-7 | 0.04 | 0.023 | 5.536E2 | 6.68E-3 |

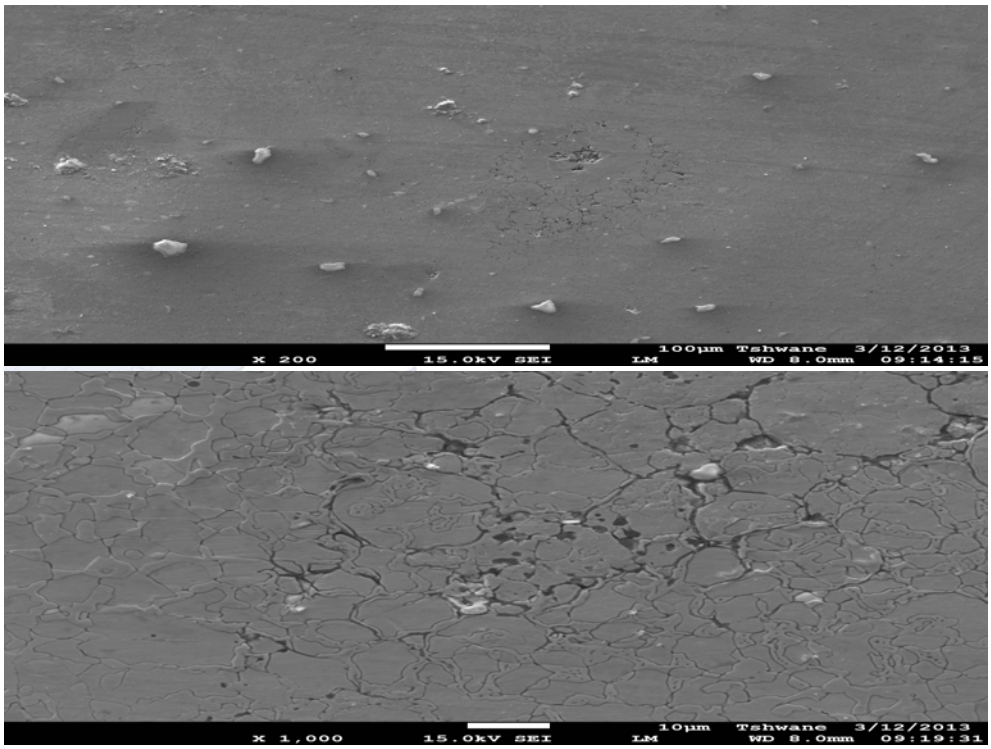


***Figure 6.*** *Typical SEM image of corroded sample in simulated mine water at different magnification*

**Discussion**

From the densification presented in Table 3, it was evident that the materials were well sintered with good densification. It was also observed that the densification of the sintered sample was increasing with percentage increase in the reinforcement. Sample 1 with 0.5% reinforcement has a densification of 99.74% while sample 5 with 2% $ZrO_2(Y_2O_3)$ has a densification of 99.87%. This was possibly due to good wettability of Zr with Fe which is in agreement with [7, 9]. The effect of Cr and Ni also contributed to the densification obtained as shown in Figure 1. Considering the features of Cr, its hardness and abrasiveness tend to reduce densification [1, 9] but rather, promote pores formation. The presence of Ni as one of the alloying elements, considering it's melting point, acts as a binder and thus try to bind the grains/powder particles of the composite, thereby reducing the porosity. This was influenced by the percentage composition of the Ni to Cr present in the composite. The basic mechanisms include; vapour transport and surface, volume and grain boundary diffusion. This vapour transport and surface diffusion mechanisms bonding affect pore rounding but not densification. This was evident in samples 2 and 3 respectively. The presence of $Y_2O_3$ as a

stabilizer in the reinforcement also influences the densification [11-12].

PM steels usually posses' residual porosity and heterogeneous microstructure, which arises from inhomogeneous distribution of alloying powders [10-12]. There were observations of pores in the SEM images of the sintered specimens (Figure 2) but distributions and sizes differ, which is one of the characteristics of sintered specimen from PM on the basis of their primary particle size and material density [13]. Figure 1 obtained from SEM represent powder particle shapes, sizes and distribution. The shapes are spherical comprising of smaller and bigger sizes which are evenly distributed within the matrix. From the EDS analyses, the expected elemental compositions were detected. EDS results show that Fe contents is the largest and appeared as spherical and grey particle. Cr and Ni were also detected though, Ni has low content. Admix were also characterized, the EDS analyses revealed all the detected elemental components. From the EDS results of all admix, yttria was not detected possibly due to its low content. Fairly enough, the distribution of the ceramic oxide was even and this gives the heterogeneous structure obtained in all the structures.

The expected balance of austenitic and ferritic phases was observed in the sintered as shown in Figure 2. The light parts were the austenitic phase while the dark patches were the ferritic. Pores, identified by the black spots, were also observed. This is evident of PM. From the SEM micrographs, it was observed that introduction of alloying elements help reduces the pore percentage present though, the pores continue to be on the rise with further addition of the ceramic oxide. This was balanced with further addition of the selected alloying elements which contain Ni, given that Ni has lower melting point, it was able to melt and flow in the matrix thereby filling up pores. There was also grain refinement by the ceramic oxide coupled with prevention of grain growth, the reinforcement ($ZrO_2(Y_2O_3)$) has different crystallographic orientations, as such, grain boundaries arises. During sintering, when pressure is applied, slip motion takes place. Grain boundaries then act as an impediment to pores movement [14].

The results of density measurement revealed that the consolidation conditions gave a higher densification. The higher density observed in bulk sample with reduction in porosity could be due to slow but steady movement of powder particles in the loose spaces under the influence of external compaction force which promotes particle to particle contact [15-17] . The identification of the adhesion mechanism in ceramic/metal interfaces suggest that they have good adhesion with each other [18] which further facilitates good densification.

Table 3 shows that densification is a function of reinforcement; i.e. densification was increasing with percentage increase in the reinforcement [19]. The achieved results were possible due to good wettability of Zr with Fe [7; 9]. Cr and Ni addition also contributed to the densification obtained.

The XRD result (Figure 3) showed that there was no existence of secondary phase. More so, the XRD diffractogram of the sintered as received 2205 and its composites show that the processing method used in this study did not encourage oxidation.

The open circuit potential (OCP) curves for ODS DSS 2205 (Figure 4) displayed similar behaviour for all the MMC samples. There was initial shift in the more negative potential i.e. the active region for the first few seconds, after which there was slight shift back to the more positive region, an indication of passivation. The potential then stabilized, this was maintained for almost all the period of the experiment. However, sample A1 showed the most negative potential followed by sample X (sintered as-received) while sample A2 has the most positive potential. The indication of this was that sample A1 has the most corrosion susceptibility followed by the as-received 2205 (X). Other samples; A2, A3 and A4 are less corrosion susceptible than sintered as-received 2205 in simulated mine water. Sample A5 on the other hand, at the initial stage of the experiment showed higher potential but over time, shifted to a lower potential compared with sample X.

Addition of PSZ with Chromium and Nickel to 2205 DSS have influence on the polarization potential by shifting the potentials into the more positive region as can be observed for samples A1, A2 and A5 in Figure 4, however, for samples A3 and A4, the potentials were shifted in to the active region which indicated that corrosion susceptibility of samples A3 and A4 are higher than that of samples A1, A2 and A5. From the graphs, it was seen that sample A5 has the highest potential with the most shift in the positive potential.

Figure 5 is the Potentio dynamic polarization results for 2205 DSS composites in simulated mine water. The polarization curves revealed the corrosion potential of each composite of 2205 and its composites. Taking composite X as the referential point; the potential of composite A1 was shifted in the more negative potential while A3 and A4 were slightly shifted in the more negative potential but A2 was almost the same with composite X. Possibility of this was that the incorporation of the dispersant (PSZ) has destabilize the balance of the original composition of the 2205 DSS in A1 and there was no further addition of Cr to affect positively the corrosion properties as shown in the corrosion current density.

However, for composite samples A2, A3 and A4, though there were further incorporation of Cr and Ni, the Cr present might not be adequate to maintain the balance in the chemical composition or inhomogeneity in the composite or even combination of both as also revealed in the SEM images**.** For composite A5, the potential was shifted in the more positive potential. The implications of this was that A5 with the most positive potential has the least susceptibility to corrosion while sample A1 with the least potential has the highest susceptibility to corrosion. Similar trend were observed from the corrosion current density which indicated that composite A5 has the least corrosion rate; A5 has the least corrosion rate as shown in Table 4. This could be connected to the percentage of Cr and Ni present in the composite matrix (2.4% Cr and 0.56% Ni). This clearly demonstrated that the Cr present in this composite is well enough to convert all the available carbon to carbide thereby suppressing the corrosion reaction rate as indicated from the current density shown from Figure 6 [5]. However, in sample A4, the Cr present is enough also to convert the carbon to carbide but the corrosion reaction might have been influenced by inhomogeneity due to high percentage of PSZ (3%). Also from the curves, there were region of passivation. However, there was no clear cut pitting potential revealed from the curves.

From the potentio-dynamic polarization scan of 2205 composites in simulated mine water, sample A5 has the highest corrosion potential (lowest corrosion susceptibility) which translated to lowest corrosion activity. This was revealed from the SEM image of the corrosion damaged surface of all the samples. Sample A5 had the least damaged surface. This confirmed that Cr inclusion in sample A5 is enough for carbon conversion to carbide thereby leading to reduction of corrosion activity. Samples A3 and A4 have the most damaged surface of all the 2205 ODS DSS in simulated mine water. This indicated that Cr might not be enough, coupled with possibility of inhomogeneous powders during mixing as sample A4 can be said to have enough Chromium addition yet, it was affected [15]. However, the attack of the simulated mine water on the ODS DSS composites was not that serious on the corrosion of the ODS DSS composites as revealed by the SEM images, Figure 6; the surfaces were not severely damaged. This demonstrated that oxide dispersion strengthening with chromium addition with Nickel can enhance corrosion property of DSS composites.

## Conclusions

The final microstructures of the composites were found to be a function of the reinforcement and the alloying elements. Densification were further enhanced by the Ni addition which is characterized by a lower melting point and was able to melt and fill up the residual pores generated within the composite created by Zirconia and Chromium.

Results also revealed the surface imaging capability of SEM for understanding corrosion as it revealed important surface information on the mechanisms of damage.

## Acknowledgements

The authors wish to acknowledge the financial support received from Tshwane University of Technology (TUT), Pretoria, South Africa, National research Foundation (NRF) South Africa and the Federal University of Technology, Akure (FUTA). The authors thank R. Tabane and Meswi K.K. for the help in the experiments.

## References

1. Olmos L., Martin Christophe L., Bouvard D., *Sintering of Mixtures of Powders: Experiments and Modelling,* Powder Technology, 2009, 190, p. 134-140.
2. Chen Z., Takeda T., Ikeda K., Murakami T., *The Influence of Powder Particle Size on Microstructural Evolution of Metal-Ceramic Composite,* Scripta Matter, 2000, 43, p. 1103-1109.
3. Chaim R, Shlayer A, Estournes C, *Densification of nanocrystalline Y2O3 ceramic powder by spark plasma sintering,* , J Eu Ceram Soc, 2009, 29, p. 91-98.
4. Karak S. K., Vishnu C. S., Witczak Z., Lojkowski W., Dutta Majumdar J., Manna I., *Studies on wear behaviour of nano-$Y_2O_3$ dispersed ferritic steel developed by mechanical alloying and hot isostatic pressing,* Wear, 2010, 270, p. 5-11.
5. Reddy K. M., Mukhopadhyay A., Basu B., *Microstructure-mechanical-tribological*

*property correlation of multistage spark plasma sintered tetragonal $ZrO_2$, J Eur Cera Soc*, 2010, 30, p. 3363-3375.

6. Glage A., Weigelt C., Rathel J., Biermann H., *Fatigue behaviour of hot pressed austenitic TWIP steel and TWIP steel/Mg-PSZ composite materials*. International Journal of Fatigue, 2014, 65, p. 9-17.
7. Sebo P., Kavecky S., Stefanik P. *Wettability of Zirconia-coated carbon by aluminium*, J Mater Sci Letters, 1994, 13, p. 592-593.
8. Muolo M.L., Passerone V.A., Passerone D., *Oxygen influence on ceramics wettability by liquid metals Ag/α-Al2O3- Experiments and Modelling*, Mater Sci and Eng, 2008, 3(495), p. 153-158.
9. Passerone A., Muolo M. L., Novakovic R., Passerone D., *Liquid matel/ceramic interactions in the (Cu, Ag, Au) / $ZrB_2$ systems*, J Eu Ceram Soc, 2007, 27, p. 3277-3285.
10. Wei D., Dave R., Pfeffer R., *Mixing and characterization of nanosized powders: An accessment of different techniques*, J Nanoparticle Research, 2002, 4, p. 21-41.
11. Chawla N., Chawla K. K., *Metal matrix composites*.: *Springer*, 2006, New York.
12. Liu Y. B., Lim S. C., Lu L., Lai M.O., *Recent development in the fabrication of metal matrix-particulate composites using powder metallurgy techniques*., J Mater Sci, 1994, 29, p. 1999-2007.
13. Li W., Gao L., *Rapid sitering of nanochrystalline $ZrO_2$(3Y) by spark plasma sintering*., J Eu Ceram Soc, 2000, 20, p. 2441-2445.
14. Ji G., Grosdider T., Bozzolo N., Launois S., *The mechanisms of microstructure formation in a nanostructured oxide dispersion strengthened FeAl alloy obtained by spark plasma sintering*. Intermetallics, 2007, 15, p. 108-118.
15. Maung A.T., Gupta M., *Microstructural, physical and mechanical characteristics of bulk nanocrystalline copper synthesized using powder metallurgy method.* Journal of Material Science Technology, 2003, 19, p. 1473-1477.
16. Sun X., Reglo R., Sun X., Yacaman M. J., *Microhardness of bulk and higher density nano crystalline copper obtained by hot compaction.* Material Chemistry Physics, 2000, 63, p. 83-87.
17. Gupta M., Tay A.A.O., Vaidyanathan K. Srivatsan T.S., *An investigation of the synthesis and characterization of copper samples for use in interconnect applications*. Material Science and Engineering, 2007, 454-455, p. 690-694.

18. Moyal J. S., Lopez-Esteban S., Pecharroma'n C., *The challenge of ceramic/metal microcomposites and nanocomposites.* Progress in Material Science, 2007, 52, p. 1017-1090.
19. Olaniran O., Olubambi P.A., Potgieter B. Olaniran B., Adegbola A. Folorunso D., *Corrosion behaviour of PM ODS composite sintered in argon atmosphere*, Journal of Materials Science and Technology, 2013, 21(3), p. 186-193.